THE JOURNAL OF PHYSICAL CHEMISTRY C

Article

pubs.acs.org/JPCC

A Distance Dependence to Lateral Self-Exchange across Nanocrystalline TiO_2. A Comparative Study of Three Homologous $Ru^{III/II}$ Polypyridyl Compounds

Brian N. DiMarco,[†,§] Tyler C. Motley,[†,§] Ryan S. Balok,[†] Guocan Li,[†] Maxime A. Siegler,[‡] Ryan M. O'Donnell,[†,∥] Ke Hu,[†] and Gerald J. Meyer*[,†]

[†]Department of Chemistry, University of North Carolina at Chapel Hill, Chapel Hill, North Carolina 27599, United States

[‡]Department of Chemistry, Johns Hopkins University, 3400 North Charles Street, Baltimore, Maryland 21218, United States

Supporting Information

ABSTRACT: Self-exchange intermolecular $Ru^{III/II}$ electron transfer, a process commonly referred to as "hole-hopping", is of great interest as it provides a means of charge transport across the surface of nanocrystalline (anatase) TiO_2 mesoporous thin films without the loss of free energy. This process was characterized by cyclic voltammetry and chronoabsorptometry for three homologous Ru diimine compounds of the general form $[Ru(LL)_2(dcbH_2)](PF_6)_2$, where LL is 2,2′-bipyridine (**bpy**), 4,4′-dimethyl-2,2′-bipyridine (**dmb**), or 4,4′-di-*tert*-butyl-2,2′-bipyridine (**dtb**) and $dcbH_2$ is 2,2′-bipyridyl-4,4′-dicarboxylic acid. Apparent electron diffusion coefficients, D, abstracted from this data increased with **dtb** < **bpy** < **dmb**. Both techniques were consistent with this trend, despite differences in the magnitude of D between the two methods. Temperature dependent measurements revealed an activation barrier for electron self-exchange of 250 ± 50 meV that was within this error the same for all three diimine compounds, suggesting the total reorganization energy, λ, was also the same. Application of Marcus theory, with the assumption that the 900 ± 100 meV total reorganization energy for self-exchange electron transfer was independent of the Ru compound, revealed that the electronic coupling matrix element, H_{AB}, followed the trend **dtb** (0.02 meV) < **bpy** (0.07 meV) < **dmb** (0.10 meV). The results indicate that insulating side groups placed on redox active molecules can be utilized to tune the electronic coupling and hence self-exchange rate constants without significantly altering the reorganization energy for electron transfer on TiO_2 surfaces.

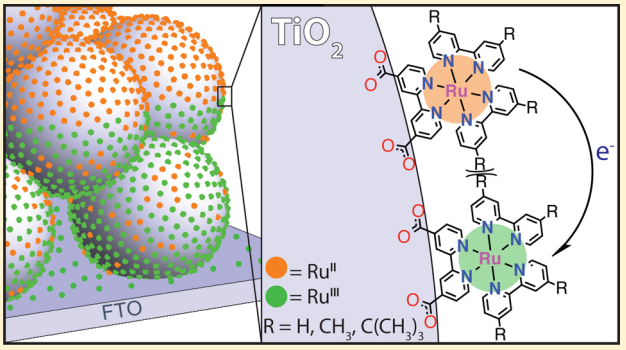

Studies as far back as 1998 have demonstrated that molecules anchored to the mesoporous nanocrystalline (anatase) TiO_2 thin films commonly used in dye-sensitized solar cells can be reversibly oxidized and reduced in standard electrochemical cells.[1,2] Molecules with formal reduction potentials that lie within the forbidden 3.2 eV band gap of TiO_2 are rapidly and quantitatively oxidized, indicating that the redox chemistry does not involve the conduction or valence bands. Instead, a model was proposed wherein electron transfer was initiated at the transparent conductive oxide substrate that supports the thin film and continues across the TiO_2 nanocrystallites by lateral intermolecular self-exchange electron transfer, now commonly referred to as "hole hopping".[1,3] A simplified description of $Ru^{III/II}$ self-exchange for three Ru compounds linked to a single TiO_2 nanocrystallite on a fluorine-doped tin oxide (FTO) substrate is given in Scheme 1. A more realistic description would display about 500 Ru compounds anchored to each ∼20 nm anatase crystallite interconnected in an ∼5 μm thin film. The importance of self-exchange electron *transfer* between surface immobilized molecules is that it provides a means to *transport* charge across nanocrystalline surfaces without a loss of free energy. Here it is shown for the first time that such transport can be controlled at the molecular level with insulating organic functional groups.

It was previously found that a threshold surface coverage of the redox active molecules was required for complete oxidation and reduction.[1] At least 50% of the saturation (often assumed to be a monolayer) surface coverage was necessary to ensure that all of the surface anchored molecules could be electrochemically accessed.[1,4] This minimum surface coverage, termed a percolation threshold, helped demonstrate that oxidation occurs through electron self-exchange, rather than physical diffusion of the anchored molecules. More recent chronoamperometric studies have provided apparent electron diffusion coefficients (D) for lateral self-exchange for a growing number of redox active molecules.[3,5−10] From this prior work, it is clear that self-exchange dynamics on TiO_2 nanocrystallites can, in some particular cases, be controlled at the molecular level. For

Received: May 2, 2016
Revised: June 7, 2016
Published: June 9, 2016

DOI: 10.1021/acs.jpcc.6b04438
J. Phys. Chem. C 2016, 120, 14226−14235

Scheme 1. Illustration of Lateral Intermolecular Self-Exchange Electron Transfer across Anatase TiO_2 Nanocrystallites Initiated at the Fluorine-Doped Tin Oxide (FTO) Substrate

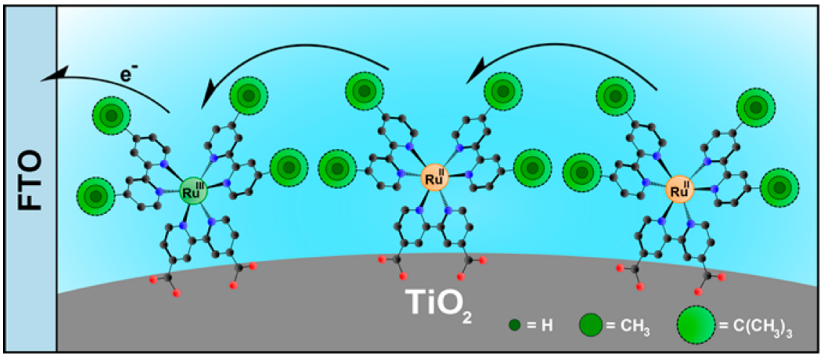

example, the inclusion of two isothiocyanate groups in a *cis*-geometry about the ruthenium center has been demonstrated to significantly increase D.[6] However, the extent to which self-exchange rate constants, and hence charge transport, across nanocrystalline surfaces can be controlled by molecular structures remains uncertain. This is unfortunate as recent studies have shown that dye-sensitized solar cells do not require mediators such as iodide and can instead use self-exchange electron transfer to complete the circuit and generate electrical power.[11] Lateral self-exchange also has relevance for the photo-oxidation of water to oxygen by molecular catalysts.[3,12] This manuscript seeks to identify structure−property relationships for self-exchange "hole hopping" in a family of three Ru polypyridyl compounds.

Nonadiabatic Marcus theory has been extensively used to quantify and predict electron-transfer rate constants[13,14] such as self-exchange electron-transfer reactions in homogeneous fluid solutions. A generic potential energy diagram for self-exchange electron transfer is shown in Figure 1. A key feature of self-exchange electron-transfer reactions is that $\Delta G^\circ = 0$, due to the equivalence of the products and reactants. The reactant and product surfaces are split at their intersection by 2 H_{AB}, the electronic coupling matrix element. For outer-sphere bimolecular self-exchange in fluid solution, electronic coupling in the encounter complex is weak, $H_{AB} \ll kT$. Constraining molecules undergoing self-exchange electron transfer to a surface is expected to further decrease H_{AB}, justifying the use of nonadiabatic Marcus theory.

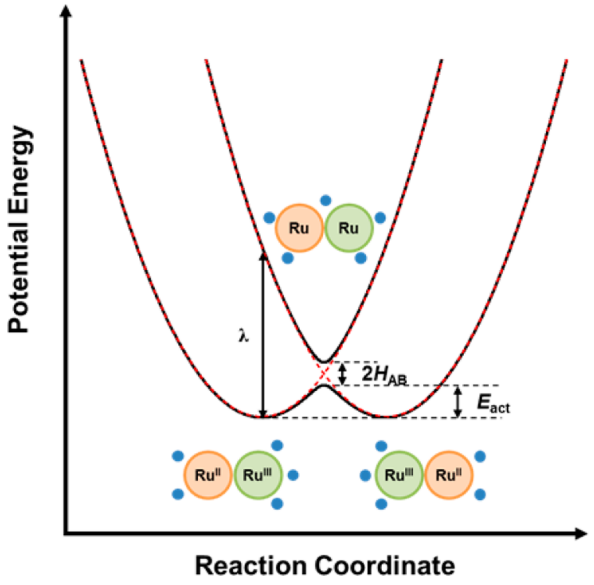

Figure 1. Reaction coordinate for nonadiabatic (dashed lines) or adiabatic (solid lines) self-exchange electron transfer reaction. The orange and green spheres represent Ru molecules in the encounter complex before, during, and after electron transfer. The blue spheres depict counterions and exaggerates their location and movement during the electron transfer process.

The self-exchange electron transfer rate constant, k_{SE}, is described by eq 1.

$$k_{SE} = \left(\frac{2\pi}{\hbar}\right)\left(\frac{|H_{AB}|^2}{\sqrt{4\pi\lambda k_b T}}\right)\exp\left(-\frac{\lambda}{4k_b T}\right) \quad (1)$$

This equation relates k_{SE} to temperature (T), H_{AB}, and the total reorganization energy (λ) for the reaction. The total reorganization energy is related to the free energy of activation ($\Delta G^{\ddagger}$) = $\lambda/4$ and is typically partitioned into inner sphere, λ_I, and outer sphere, λ_O, components, $\lambda = \lambda_I + \lambda_O$. Inner-sphere reorganization reflects changes in bond lengths and angles that accompany electron transfer, while λ_O reflects reorientation of the solvent molecules and ions present in the electrolyte.

The state of the art in characterization of lateral self-exchange in mesoporous TiO_2 thin films was recently reported by Moia and co-workers.[5] These authors quantified self-exchange among 10 different dye molecules as a function of temperature for the first time. Self-exchange was found to be an activated process with E_{act} that ranged from 170 to 370 meV, values that were dependent on the nature of the redox active molecule. A Marcus analysis yielded λ and H_{AB} for self-exchange in macrocyclic, ruthenium polypyridyl, and organic push−pull (i.e., D−π−A) molecules. The λ's abstracted from the transient kinetic data were found to be in good agreement with expectations based on density functional theory. Reorganization energies associated with highly delocalized frontier orbitals and rigid molecular structures with extended conjugation were concluded to be small. There was also some evidence that nonconjugated functional groups on the molecules could potentially influence lateral self-exchange. This report compliments this previous study through characterization of a homologous series of compounds where λ is expected to be held near parity, yet the steric bulk of the bipyridine ligand was intentionally varied. The data provide compelling evidence that these side groups can be used to tune the self-exchange between immobilized redox sites.

DOI: 10.1021/acs.jpcc.6b04438
J. Phys. Chem. C 2016, 120, 14226−14235

Herein a comparative study of three analogous Ru diimine compounds of the general form $[Ru(LL)_2(dcbH_2)](PF_6)_2$, where $dcbH_2$ is 2,2′-bipyridyl-4,4′-dicarboxylic acid and LL is 2,2′-bipyridine (**bpy**), 4,4′-dimethyl-2,2′-bipyridine (**dmb**), or 4,4′-di-*tert*-butyl-2,2′-bipyridine (**dtb**), is reported, Scheme 2.

Scheme 2. Chemical Structure of the Molecules Studied

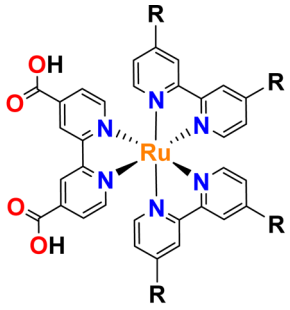

bpy	**R = H**	**$[Ru(bpy)_2(dcbH_2)](PF_6)_2$**
dmb	**R = CH_3**	**$[Ru(dmb)_2(dcbH_2)](PF_6)_2$**
dtb	**R = $C(CH_3)_3$**	**$[Ru(dtb)_2(dcbH_2)](PF_6)_2$**

These compounds share a tris-chelated, pseudo-octahedral geometry, and hence, the reorganization energy for the $Ru^{III/II}$ redox chemistry is expected to be approximately the same across the series. Each compound possesses a single dcb ligand for surface binding to TiO_2 with two other substituted bipyridine ligands possessing substitutions at the 4,4′-position that were expected to influence lateral self-exchange reactivity. In fact, small changes to the molecular structure, such as replacement of a H atom with a methyl group, were found to have a surprisingly large influence on *D*, as observed through both chronoabsorptometry and temperature-dependent cyclic voltammetry studies.

METHODS

Materials. The following solvents and reagents were purchased from the indicated supplier and were used without further purification: titanium(IV) isopropoxide ($Ti(i\text{-}OPr)_4$; Aldrich, ≥97.0%); deionized water; acetonitrile (CH_3CN, Burdick and Jackson, spectrophotometric grade); diethyl ether (Et_2O; Fisher Scientific, 99.9%); anhydrous ethanol (EtOH, Fisher Scientific, 99%); silver nitrate ($AgNO_3$; Stream, 99.9%); sodium hydroxide (NaOH; Sigma-Aldrich, >97%); hexafluorophosphonic acid (HPF_6; 65% solution in H_2O, Sigma-Aldrich); lithium perchlorate ($LiClO_4$; Sigma-Aldrich, 99.99%); ammonium hexafluorophosophate (NH_4PF_6; Sigma-Aldrich, 99.8%); 4,4′-dimethyl-2,2′-bipyridine (dmb; Combi-Blocks); argon (Airgas, ≥99.998%); oxygen (O_2, Airgas, ≥99.998%); fluorine-doped tin(IV) oxide (FTO; Hartford Glass Co., Inc., 2.3 mm thick, 15 Ω/□); $[Ru(bpy)_2(dcbH_2)](PF_6)_2$ (**bpy**; Solaronix). The complexes [(*p*-cymene)Ru(deeb)Cl]Cl, where deeb is the 2,2′-bipyridyl-4,4′-diethyl ester, and $[Ru(dtb)_2(dcbH_2)](PF_6)_2$ (**dtb**) were available from previous studies.[15,16] Anion metathesis of **dtb** was used to generate a ClO_4^- salt. Single crystals of the perchlorate salt of **dtb** suitable for X-ray structure determination were obtained by slow diffusion of hexanes into concentrated acetonitrile solutions.

Synthesis. *$[Ru(dmb)_2(deeb)](PF_6)_2$ (**1**).* The [(*p*-cymene)-Ru(deeb)Cl]Cl (80.1 mg, 0.13 mmol) precursor was combined with dmb (49.0 mg, 0.27 mmol) and $AgNO_3$ (61.6 mg, 0.36 mmol) in 10 mL of EtOH. The solution was purged with N_2 for >15 min and then heated to a reflux under a N_2 atmosphere for 14 h. After this time had elapsed, the solution was cooled to room temperature and the solvent was removed. The colored product was redissolved in a minimal amount of water. The aqueous solution was filtered to remove any remaining Ag^+ salts. To the filtrate was added an excess of NH_4PF_6, which yielded a brown solid. The solid was filtered and dissolved in dichloromethane to prevent any remaining Ag^+ salts from being carried forward. The solvent was removed, and the product was dissolved in CH_3CN. Slow diffusion of Et_2O into a concentrated CH_3CN solution afforded 128.3 mg of product as large brown crystals, which were suitable for X-ray structure determination (yield = 92%). ^1H NMR (400 MHz, CD_3CN) δ 9.00 (s, 2H), 8.334 (d, J = 6.2 Hz, 4H), 7.94 (d, J = 5.8 Hz, 2H), 7.80 (d, J = 5.9 Hz), 7.50−7.43 (M, 4H), 7.26−7.18 (M, 4H), 4.24 (q, J = 6.9, 14.1, 4H) 2.52 (d, J = 9.92 Hz, 12H), 1.41 (t, J = 7.1 Hz, 12H). ^{13}C NMR (150 MHz, CD_3CN) δ 164.8, 159.2, 157.5, 154.0, 152.3, 152.1, 152.1, 151.8, 139.6, 129.7, 129.6, 127.6, 126.3, 124.8, 63.9, 21.6, 14.6. HS-ESI-MS: m/z = 915.1826 (calcd for $RuC_{40}H_{40}N_6O_4PF_6$ $[Ru(dmb)_2(deeb)]-(PF_6)^+$: 915.1796); m/z = 385.1077 (calcd for $RuC_{40}H_{40}N_6O_4$ $[Ru(dmb)_2(deeb)]^{2+}$: 385.1077).

*$[Ru(dmb)_2(dcbH_2)](PF_6)_2$ (**dmb**).* $[Ru(dmb)_2(deeb)](PF_6)_2$ (60.9 mg, 57 μmol) and NaOH (9 mg, 230 μmol) were added to 30 mL of a 1:5 EtOH/H_2O solution. The solution was purged with N_2 for >20 min and then heated to reflux. The reflux was maintained for 15 h under a N_2 atmosphere, after which the solution was allowed to cool to room temperature. The solution volume was reduced, and the remaining water was acidified with HPF_6. The resulting solid was filtered, washed with Et_2O and H_2O, and left under a vacuum overnight to dry. This afforded 51.1 mg of a reddish brown solid (yield = 88.6%). ^1H NMR (500 MHz, CD_3CN) δ 9.52 (s, 2H), 8.33 (d, J = 8.1 Hz, 4H), 7.82 (dd, J = 5.8, 21.5 Hz, 4H), 7.48 (dd, J = 5.8, 21.1 Hz, 4H), 7.24 (d, J = 5.2 Hz, 2H), 7.17 (d, J = 5.7 Hz, 2H), 2.51 (d, J = 14.2 Hz, 12H). ^{13}C NMR (150 MHz, CD_3CN) 167.3, 159.4, 157.7, 157.6, 153.3, 152.2, 151.8, 129.62, 129.60, 128.0, 126.25, 126.22, 21.6. HS-ESI-MS: m/z = 859.1162 (calcd for $RuC_{36}H_{32}N_6O_4PF_6$ $[Ru(dmb)_2(dcbH_2)](PF_6)^+$: 859.1142); m/z = 357.0758 (calcd For $RuC_{36}H_{32}N_6O_4$ $[Ru(dmb)_2(dcbH_2)]^{2+}$: 357.0764).

Thin Film Preparation. Titania nanocrystallites were made by hydrolysis of $Ti(i\text{-}OPr)_4$ via a previously published sol−gel technique.[2] Thin, mesoporous films were cast through doctor blading onto an ethanol cleaned FTO substrate using Scotch tape (~50 μm thick) as a spacer for consistent thickness. The films were first dried while covered for 30 min and then sintered at 450 °C for 30 min under O_2 flow at ~1 atm. Films were either used immediately or stored in an oven (~70 °C) until use. Film thicknesses (~4−6 μm) were determined using a Bruker Dektak XT profilometer using the Vision 64 software.

Titania films were submerged into concentrated CH_3CN solutions of **bpy**, **dmb**, or **dtb** to allow the molecules to anchor to the nanocrystallite surface. Films were submerged for a minimum of 48 h to ensure saturated surface coverages. Prior to use, the films were soaked for ~1 h in neat CH_3CN to remove any weakly adsorbed molecules from the film in order to minimize dye desorption during the course of the experiments.

UV−Visible Spectroscopy. Steady-state UV−visible spectra were obtained on either a Hewlett-Packard 8453 photo-

DOI: 10.1021/acs.jpcc.6b04438
J. Phys. Chem. C 2016, 120, 14226−14235

diode array or a Varian Cary 60 spectrophotometer at room temperature. All measurements were made in custom-made 1 cm path length quartz cuvettes with a 24/40 ground glass joint affixed to the top. Surface-functionalized films were placed along the diagonal of the cuvette at a 45° angle to the incident probe beam.

Electrochemistry. Electrochemical measurements were performed with a potentiostat (Bioanalytical Scientific Instruments model CV-50W or Epsilon electrochemical analyzer) using a standard three-electrode arrangement. A surface-functionalized TiO_2 film was employed as the working electrode, while a platinum mesh was used as the auxiliary electrode. Potentials were applied against a nonaqueous silver wire pseudoreference electrode (Pine Research Instruments), which was filled with 0.1 M $LiClO_4$ containing CH_3CN. Unless otherwise noted, the pseudoreference electrode was externally calibrated against the ferrocenium/ferrocene ($Fc^{+/0}$) reduction potential in 0.2 M $LiClO_4$ containing CH_3CN, where the $Fc^{+/0}$ potential is 0.31 V vs the saturated calomel electrode (SCE) and SCE is 0.241 V vs the normal hydrogen electrode (NHE).[17] The three electrodes were placed within a custom quartz cuvette, consisting of a 1 cm path length square quartz cuvette attached by ∼8 cm of round glass tubing to a 24/40 ground glass joint, which allowed the TiO_2 film to be monitored spectroscopically. The electrode connections were fed through a rubber septum, which was used to seal the cuvette. For measurements taken at room temperature, the $Fc^{+/0}$ potential was measured before and after the experiment to ensure reference electrode stability.

Spectroelectrochemical measurements were used to quantify $E°$ for TiO_2 anchored complexes. The experiment monitored the absorbance of the surface-functionalized TiO_2 film while applying increasingly positive electrochemical biases. The films were held at each potential for a minimum of 1 min, or until no additional spectral changes were observed, in order to ensure the film was equilibrated. Chronoabsorptometry (CA) was used to investigate the apparent diffusion coefficient, D, for the molecules studied. In contrast to the spectroelectrochemical experiment, a single oxidizing potential was applied to the film, and the oxidation rate was monitored spectroscopically as a function of time. Full oxidation of the film was achieved after stepping the potential to $E°$ + 0.5 V for several minutes. A new surface-functionalized film was used for each experiment to minimize the impact of dye desorption. All spectroelectrochemical experiments were performed in argon purged CH_3CN containing 0.1 M $LiClO_4$ as the supporting electrolyte.

Cyclic voltammetry (CV) was also used to investigate D for the surface bound compounds. Variable temperature CV experiments were performed within a custom cell comprised of an ∼1 cm^2 square tubing attached to a 19/22 ground glass joint. The electrodes were arranged in a manner analogous to the CA experiments. The argon purge electrochemical cell was placed within a UniSoku CoolSpek USP-203-B liquid nitrogen cryostat, which allowed the temperature to be adjusted to ±1 °C of the desired temperature. The apparatus was allowed to thermally equilibrate at each temperature for >10 min prior to performing the measurement. Again, a new film was used for each experiment. Note that D_{CV} and D_{CA} denote diffusion coefficients that were measured by CV or CA, respectively.

Data Analysis. Kinetic modeling was performed in Origin 9.0, and least-squares error minimization, accomplished by the Levenberg−Marquardt iteration method. Resulting values from the best fit are reported with the standard error from the fitting procedure. In the case of the CA measurements, the error reported is the standard deviation of multiple trials. Spectral modeling of the spectroelectrochemical data was performed as a least-squares fitting function written into a custom script in Mathematica 9.

Calculation of c_0 and R. The "concentration" of redox active molecules within the mesoporous TiO_2 thin films is an ill-defined parameter. To determine the volume concentration (cm^{-3}), c_0, and, consequently, the intermolecular spacing between ruthenium compounds (cm), R, assumptions about the porosity of the film and close packed nature of the molecules were required. Below are presented methods to determine the upper and lower limits as well as one intermediate value of R.

Upper Limit of R. This approach represents an upper limit to R as the molecules are assumed to be distributed throughout both the TiO_2 nanoparticle and pore volume as opposed to the more reasonable situation where they are localized on the TiO_2 surface. Further calculations of R in this regime lead to upper limits for both the self-exchange rate constant and the electronic coupling matrix element, Table S1. To estimate c_0 and R, the surface coverage (mol/cm^2), Γ, was first determined with eq 2, where A and ε are the absorbance and molar extinction coefficient (M^{-1} cm^{-1}) of the film at a given wavelength and 1000 is a factor to convert from L to cm^3. Note that the wavelength used for each compound is the wavelength where the absorbance of the surface-functionalized TiO_2 film is the same in neat and 0.1 M $LiClO_4$ solutions in acetonitrile (*vide infra*). The extinction coefficient at the absorbance peak observed in fluid solution is assumed to be retained upon anchoring.

$$A = 1000 \times \varepsilon \times \Gamma \tag{2}$$

Next, Γ was converted to c_0 using eq 3, where N is Avogadro's number and d is the film thickness (cm). The inclusion of cos(45°) adjusts for the path length of the probe being incident to the film at 45°. The Ru compounds were assumed to be distributed evenly throughout the total film volume.

$$c_0 = \frac{\Gamma \times N}{d \times \cos 45°} \tag{3}$$

Finally, to convert to R, the cubic lattice arrangement was assumed on the surface as was done previously by Daum et al. for redox sites immobilized in polymer films[18] and by Moia et al. for molecules anchored to TiO_2 films.[5] This relation is given simply by eq 4.

$$R = {c_0}^{-1/3} \tag{4}$$

Intermediate Value of R. For a more accurate value of R, the pore volume of the mesoporous TiO_2 film must be accounted for. In the present study, the films were assumed to have an ∼50% porosity. In this method, the c_0 was calculated as it was in the upper limiting case. To adjust for the pore volume, the c_0 was multiplied by a factor of 2. This approximation still assumes that the Ru compounds are evenly distributed throughout the volume occupied by the TiO_2 nanoparticles, but now the volume has decreased by half which results in a doubling of the calculated concentration. R was calculated as before.

Lower Limit of R. The lower limit of R was estimated from crystal structures of the Ru molecules, where R represents the distance between the substituents in the four positions of the bipyridine group trans to one another (Figure 2). In order to carry out further calculations needed to determine the apparent

DOI: 10.1021/acs.jpcc.6b04438
J. Phys. Chem. C 2016, 120, 14226−14235

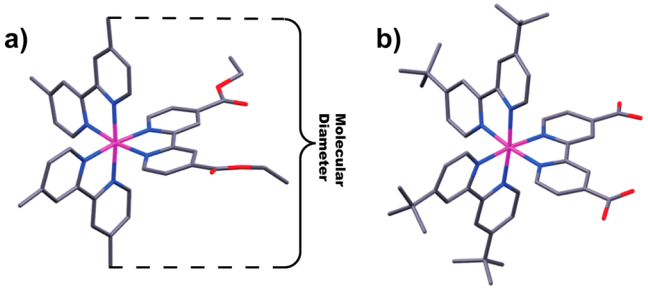

Figure 2. (a) Crystal structure of $[Ru(dmb)_2(deeb)](PF_6)_2$. (b) Crystal structure of $[Ru(dtb)_2(dcbH_2)](ClO_4)_2$. All hydrogen atoms and anions are omitted for clarity purposes. Color code: pink, Ru; blue, N; red, O; gray, C.

diffusion coefficients from the CV experiments, eq 4 was used to calculate c_0. This value gives an estimate for the spacing between molecules close to the van der Waals radii limit allowed by the compounds, and calculations based on these values lead to a lower limit for the self-exchange rate constant and electronic coupling matrix element.

RESULTS

Preparation of the $[Ru(dmb)_2(deeb)](PF_6)_2$ (**1**) precursor was achieved in high yield using a modified, previously reported procedure for the synthesis of similar ruthenium polypyridyl compounds.[15] Base catalyzed hydrolysis of the ethyl ester groups in **1** generated the desired carboxylic acid form of the compound, **dmb**. Structural identity was confirmed through ^1H and ^{13}C NMR and high-resolution mass spectroscopy.

Slow diffusion of Et_2O into concentrated CH_3CN solutions of **1** gave crystals suitable for X-ray diffraction (Figure 2). The average Ru−N distance is 2.054 Å. The Ru−N distance for the deeb ligand is slightly shorter than those for the dmb ligands, indicative of stronger back-bonding from the Ru nonbonding d-orbitals to deeb π^* orbitals. The average N−Ru−N bite angle is 78.73°, while the bite angle for the deeb ligand is 0.5° smaller than the dmb ligand, consistent with the shorter Ru−N bond lengths for the deeb ligand. The Ru compounds appear in pairs in the crystal structure through $\pi-\pi$ interaction between the deeb ligands with an interlayer distance of 4.331 Å. A weaker $\pi-\pi$ intermolecular interaction with neighboring dmb ligands was also evident in the solid state. Saponification of the ester is not expected to significantly impact the Ru−N bond distances, or the N−Ru−N bite angles. No significant structure differences were observed for $[Ru(dtb)_2(dcbH_2)](ClO_4)_2$ when compared to **1**. An average Ru−N bond length of 2.056 Å and an average N−Ru−N bite angle of 78.62° were observed.

A pertinent value for this study is the "molecular diameter", or the distance between the farthest points on the molecule. This value was taken to be the distance between substituents in the four positions of bipyridine that were trans to one another on adjacent coordinated ligands. More specifically, this is the H to H distance for **bpy**, the C to C of the methyl groups for **dmb**, or the CH_3 group to CH_3 group of the *tert*-butyl groups for **dtb**. A summary of these values and other relevant parameters for all three compounds is given in Table 1. Additional crystallographic data for **dtb** and **1** are found in the Supporting Information.

The TiO_2 thin films were reacted with the desired Ru compounds by submersion into concentrated CH_3CN solutions. Extended reaction times (>48 h) were used to ensure that maximum surface coverages were achieved. Representative spectra of the TiO_2 films placed in neat CH_3CN after surface functionalization, abbreviated TiO_2|X, are seen in Figure 3 (solid lines). The main absorption feature centered at ∼450 nm observed in neat CH_3CN is reasonably assigned as metal-to-ligand charge transfer (MLCT) transitions. It is assumed that the peak extinction coefficients, ε, are retained upon surface anchoring, Table 2.

Table 1. Selected Crystal Structure Parameters

	average Ru−N distance (Å)	average N−Ru−N bite angle (deg)	molecular diameter (nm)
bpy[a,b]	2.056	79.01	1.15
dmb[b]	2.054	78.83	1.27
dtb	2.056	78.62	1.37

[a]Taken from ref 19. [b]Values shown are for the ethyl ester complex.

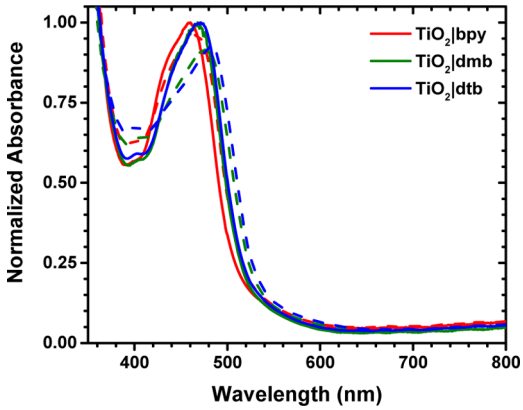

Figure 3. Normalized absorption spectra of compounds **bpy**, **dmb**, and **dtb** anchored to TiO_2 in neat CH_3CN (solid line) or in a 0.1 M $LiClO_4$ solution in CH_3CN (dashed line). The TiO_2 absorption spectrum was subtracted out from the spectra of the surface-functionalized films.

The addition of 0.1 M $LiClO_4$ to the neat CH_3CN induced a bathochromic shift of the MLCT absorption (Figure 3, dashed lines). This has previously been reported for ruthenium polypyridyl complexes, and is attributed to a change in the electric field at the surface of the TiO_2 upon cation adsorption.[20−22] The peak absorption for each compound in the presence of Li^+ is shown in Table 2. The surface coverage, Γ, was calculated using a modified Beer's law expression, Table 2.[4] Note that Γ was calculated with the assumption that the ε value measured in fluid solution was the same as that for the surface anchored molecules. Though several assumptions are made during this calculation, a comparison of values between the three compounds provides insight into the molecular environment present at the surface. A decrease in Γ was seen with increasing steric bulk, suggesting that the side groups influence the intermolecular distance.

Spectroelectrochemical measurements were performed on TiO_2|**dmb** to quantify the $E°(Ru^{III/II})$ potential. Application of a positive applied potential resulted in spectral changes consistent with oxidation of Ru^{II} to Ru^{III}, Figure 4. Complete oxidation to yield Ru^{III} was determined when an increased applied potential no longer induced a spectral change. The mole fraction, χ, of oxidized and reduced species present at a given applied

DOI: 10.1021/acs.jpcc.6b04438
J. Phys. Chem. C 2016, 120, 14226−14235

Table 2. Selected Spectral, Electrochemical, and Film Parameters for the Compounds Studied

	λ_{max}^{soln} (nm) (ε, M^{-1} cm^{-1})[a]	λ_{max}^{neat} (nm)[b]	$\lambda_{max}^{Li^+}$ (nm)[c]	E° (V vs NHE) (α)	Γ (10^{-7} mol/cm^2)	c_0 (10^{19} cm^{-3})
bpy	471 (12000)	460	467	1.48 (1.4)	1.9 ± 0.14	38 ± 2
dmb	475 (14200)	468	475	1.39 (1.6)	0.95 ± 0.20	19 ± 1
dtb	465 (16400)	471	482	1.36 (1.2)	0.77 ± 0.13	12 ± 1

[a]Peak absorption of the compound in neat CH_3CN. [b]Peak absorption of the TiO_2 anchored compound in neat CH_3CN. [c]Peak absorption of the TiO_2 anchored compound in 0.1 M $LiClO_4$ containing CH_3CN.

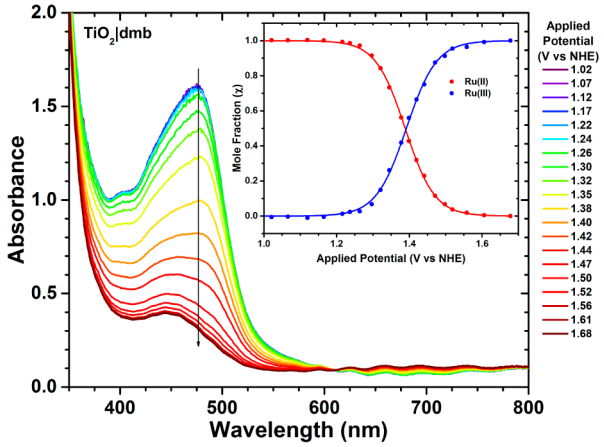

Figure 4. Spectroelectrochemical oxidation of TiO_2|**dmb** immersed in 0.1 M $LiClO_4/CH_3CN$ electrolyte. The inset plots the fraction of oxidized or reduced compound as a function of applied potential. Overlaid is a fit to a modified Nernst equation, eq 5.

potential was determined through spectral modeling using a linear combination of the Ru^{II} and Ru^{III} species.

The formal reduction potential, E°, was determined using eq 5.

$$\chi = (1 + 10^{(E_{app} - E^\circ)/(\alpha \cdot 59)})^{-1} \quad (5)$$

In this equation, E_{app} is an applied potential and α is an ideality factor that accounts for deviations from Nernstian behavior. Values for E° and α are given in Table 2. The equivalent data for **bpy** and **dtb** can be found in the Supporting Information (Figure S2 and S3).

Insight into intermolecular electron self-exchange was gained by spectroscopically monitoring the oxidation process as a function of time after a potential step ~0.5 V positive of $E^\circ(Ru^{III/II})$. A comparison of the absorbance decay monitored at a single wavelength for the three Ru compounds of interest is seen in Figure 5. The rate of this conversion was recast as the apparent electron diffusion coefficient, D_{CA}, using eq 6.[1]

$$\Delta A = \frac{2\Delta A_f D_{CA}^{1/2} t^{1/2}}{d\pi^{1/2}} \quad (6)$$

In this equation, ΔA_f is the final change in absorbance and d is the TiO_2 film thickness. A linear fit to the initial CA data allowed for the determination of D_{CA} using eq 6. The wavelengths monitored during the oxidation were 468, 480, and 482 nm for **bpy**, **dmb**, and **dtb**, respectively. During the analysis, care was taken to only fit the linear portion of the data. Deviations from linearity indicate movement away from diffusion-limited conditions, which is typical as the oxidation front approaches the edge of the film. Bonhôte and co-workers reported that linearity was maintained for the oxidation of ~60% of the molecules within the mesoporous thin film.[1] Thus, only the first 60% of the total observed absorption change was

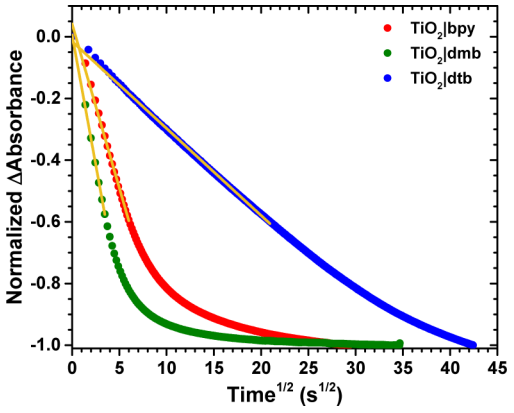

Figure 5. Normalized absorption change measured after application of a potential sufficient to oxidize the indicated compounds plotted against the square root of time. Overlaid in gold is the fit based on eq 6.

fit, gold overlay, Figure 5. The observed rate of oxidation, as well as the calculated D_{CA} value, was seen to increase following **dtb** < **bpy** < **dmb**.

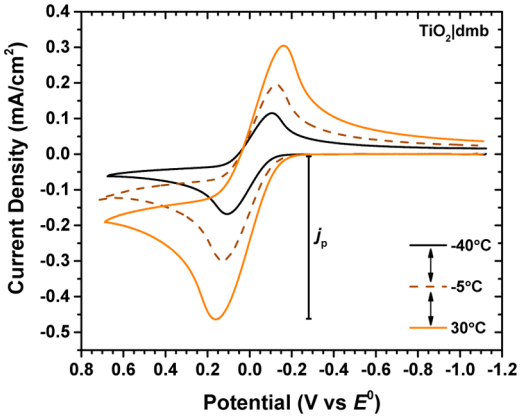

Figure 6. Representative cyclic voltammograms for **dmb** anchored to TiO_2 immersed in 0.1 M $LiClO_4$ in CH_3CN at the indicated temperatures.

The apparent diffusion coefficients were determined over a range of temperatures for each compound by cyclic voltammetry (CV), Figure 6. The peak current density, j_p, observed during the CV, was related to D_{CV} using eq 7.[5]

$$D_{CV} = \frac{5.02 k_b T j_p^{\,2}}{q^3 c_0^{\,2} \nu} \quad (7)$$

In this equation, k_b, q, T, c_0, and ν are the Boltzmann constant, the elementary charge, the temperature, the volume concentration, and the scan rate, respectively. Determination of c_0 was nontrivial, as concentrations at nanocrystalline TiO_2 interfaces

DOI: 10.1021/acs.jpcc.6b04438
J. Phys. Chem. C 2016, 120, 14226−14235

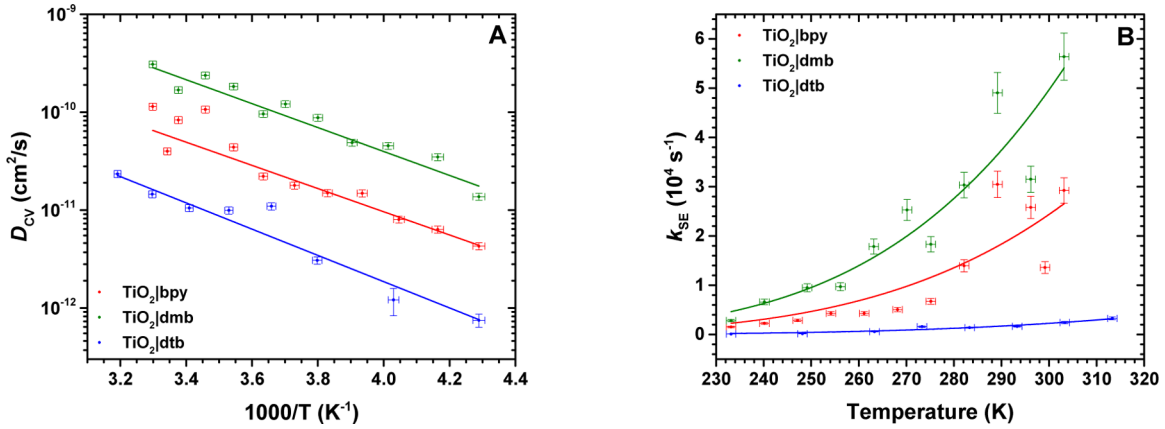

Figure 7. (A) Arrhenius plot for **bpy**, **dmb**, and **dtb** anchored to TiO_2 describing the variation of D_{CV} with inverse temperature as obtained by cyclic voltammetry. Overlaid are the best fits to the Arrhenius equation. (B) The temperature dependence of k_{SE} as described by nonadiabatic Marcus theory (overlaid curves).

Table 3. Apparent Diffusion Coefficients and Marcus Self-Exchange Parameters for Surface Anchored Ruthenium Compounds

	D_{CA} (10^{-9} cm^2/s)	D_{CV}[a] (10^{-10} cm^2/s)	E_{act} (meV)	A (10^{-7} cm^2/s)	H_{AB}[b] (meV)	R (nm)
TiO$_2$|**bpy**	2.2 ± 1.1	1.1 ± 0.1	240 ± 30	5 ± 6	0.07 ± 0.04	1.4 ± 0.03
TiO$_2$|**dmb**	5.3 ± 0.6	3.1 ± 0.2	240 ± 20	30 ± 30	0.10 ± 0.06	1.8 ± 0.03
TiO$_2$|**dtb**	0.24 ± 0.01	0.14 ± 0.01	270 ± 30	4 ± 5	0.02 ± 0.02	2.0 ± 0.06

[a]Value taken at 30 °C. [b]λ = 900 ± 100 meV shared between data sets.

are an ill-defined parameter. For the purposes of this study, the total volume available to the molecule was assumed to be the volume of the TiO_2 film, excluding pores, with the Ru molecules uniformly dispersed throughout the remaining volume. The Γ value was initially quantified using a modified Beer's law. Γ was then converted to c_0 by eq 3, where cos(45°) accounts for the increase in path length due to the film being at a 45° angle to the probe. To account for an ∼50% porosity, the calculated c_0 was multiplied by a factor of 2. Table 2 shows the c_0 obtained for the compounds studied. Other methods used to calculate c_0 are discussed in the experimental section and provided quantitatively different values of D_{CV}, yet the same trend was observed. Throughout all experiments, ν was kept to be 0.1 V/s, applied against a self-contained Ag wire. The expected temperature dependence of the reference electrode was not important to the experiment. A linear correction was made to all the data in order to compensate for nonfaradaic processes, as was described previously by Moia et al.[5] j_p was determined by dividing the observed peak current from the initial scan by the geometric area of the TiO_2 film (∼1.5 cm^2).

$$D_{CV} = Ae^{(-E_{act}/k_bT)} \tag{8}$$

Activation energies, E_{act}, for self-exchange on the surface were extracted from the variable temperature data with the Arrhenius equation, eq 8. Figure 7A shows the D_{CV} obtained over a range of temperatures fit to eq 8. E_{act} along with the associated pre-exponential factors, A, are included in Table 3. The abstracted E_{act} values were between 240 and 270 meV.

In order to perform a Marcus analysis on these data, D_{CV} was converted into an effective electron transfer rate constant, k_{SE}, using eq 9.[5] This required knowledge of the intermolecular distance, R, between redox active sites. It was assumed that the molecules were evenly distributed in a cubic lattice throughout the porosity corrected volume of the film, eq 4. Values of R for each compound are shown in Table 3. These values represent an "intermediate" estimate of the true and unknown intermolecular distance on the TiO_2 surface. Upper and lower limits of R were also established and are given in Table S1.

$$k_{SE} = \frac{4D_{CV}}{R^2} \tag{9}$$

The magnitude of H_{AB} was determined by fitting the data shown in Figure 7B to nonadiabatic Marcus theory for electron self-exchange, eq 1. To aid in the fitting process, a global fitting analysis was used and λ was shared between the three data sets. Table 3 shows the resulting H_{AB} values. As previously mentioned, the value of R utilized directly influenced the value of H_{AB} determined. Figure S1 shows the variation of H_{AB} and k_{SE} based on each method used to determine R. A summary of these parameters is found in Table S1.

DISCUSSION

As was described in the introduction section, self-exchange between surface immobilized molecules results in the transport of charge and is hence of interest for energy applications.[11] A key finding disseminated here is that insulating organic side groups on the redox active molecules can be used to tune self-exchange "hole hopping" and hence charge transport across nanocrystalline TiO_2 surfaces. This was most readily quantified by abstraction of an apparent diffusion constant, D, from the temporal data. Indeed, an experimental challenge was to identify methods by which the intrinsic self-exchange rate constants and activational parameters could be reliably abstracted from bulk kinetic electrochemical data. The two techniques utilized herein relied upon a ramped (cyclic voltammetry) or stepped (chronoabsorptometry) potential to quantify $Ru^{III/II}$ self-exchange, and while both techniques revealed the same trend in D, **dmb** > **bpy** > **dtb**, the quantitative values differed significantly. Below we discuss the electrochemical methods used to quantify self-exchange

DOI: 10.1021/acs.jpcc.6b04438
J. Phys. Chem. C 2016, 120, 14226−14235

followed by an analysis of the kinetic data within the framework of Marcus theory for nonadiabatic electron transfer.

Quantification of Reduction Potentials and Apparent Diffusion Coefficients. The formal $E°(Ru^{III/II})$ reduction potentials were taken as the equilibrium potential where equal numbers of compounds measured spectroscopically were present in the formal oxidation states of III and II. The electron donating methyl and *tert*-butyl groups in the dmb and dtb ligands induced a measurable negative shift in the formal reduction potentials relative to that measured for TiO_2|**bpy**. A complication in data analysis was the non-Nernstian behavior of the interfacial redox chemistry. An ~80 mV potential step was required to induce a factor of 10 change in the Ru^{III}/Ru^{II} ratio for **bpy**, and ~70 mV was required for **dtb** rather than the Nernstian value of 59 mV. The spectroelectrochemical data were adequately modeled by including α to account for deviation from Nernstian behavior, as has been done in the past; however, such modeling does not address the origin(s) of the nonideality. Prior studies with metalloporphyrins and molecules with two redox active groups have indicated that the nonideality arises from local electric fields present at the oxide−electrolyte interface.[23] The α increased in the order **dmb** > **bpy** > **dtb**, suggesting that intermolecular interactions like those in the Frumkin isotherm model may also underlie this behavior.[9] If instead the nonideality arises from a distribution of formal reduction potentials, then the data may reflect a greater degree of heterogeneity for **bpy** than for **dtb**. Regardless of the nonideality origin(s), the steady state spectroelectrochemical data suggests that the true self-exchange electron transfer hole-hopping may not occur with $\Delta G° = 0$ throughout the mesoporous film.

Chronoabsorptometry (CA) and cyclic voltammetry (CV) experiments were performed to estimate the diffusion coefficient, D, for self-exchange. The data analysis is based upon a semi-infinite diffusion boundary approximation that has been previously described.[5] Since the mesoporous TiO_2 thin film has a finite thickness, this analysis is only valid if the "front" of oxidized molecules does not reach the outer edge of the mesoporous thin film. This boundary condition is maintained through the CV experiments, where only about 5% of the redox active molecules within the thin film were oxidized. This value was determined by using $L = (D_{CV}*t)^{1/2}$, where L is the linear diffusion length and t is the elapsed time from the onset of oxidation to the peak oxidation current. In contrast, all of the electrochemically accessible compounds were oxidized over the course of the CA experiments, Scheme 3.

Deviation from linearity was observed when ~60% of the compounds were oxidized, which has been previously attributed to the breakdown of the boundary conditions used in deriving this equations.[24] Both experiments revealed that D decreased in the order **dmb** > **bpy** > **dtb**; however, the values abstracted from cyclic voltammetry data were consistently about an order of magnitude larger, $D_{CV} > D_{CA}$. This behavior has previously been reported and is not fully understood.[25] Since a larger fraction of the self-exchange occurs near the fluorine-doped tin oxide (FTO) substrate in the voltammetry measurements, the larger diffusion coefficient may reflect more rapid self-exchange near the FTO interface.

Values of D have previously been determined for other metal polypyridyl complexes anchored to TiO_2 surfaces, and provide context for the values reported here. Trammel and Meyer previously determined $D_{CA} = 1.4 \times 10^{-9}$ cm^2/s for the $Os^{III/II}$ self-exchange in the compound $[Os(bpy)_2(dcb)]^{2+}$.[4] This value

Scheme 3. An Idealized Representation of Three Surface Functionalized Anatase Layers on an FTO Substrate during a Chronoabsorptometry (CA) Experiment[a]

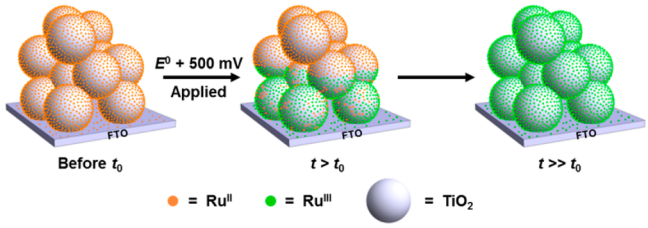

[a]At time t_0, all of the ruthenium compounds are in the formal oxidation state of II. After a potential step 500 mV more positive than the formal $E°(Ru^{III/II})$ reduction potential, the FTO substrate oxidizes the Ru^{II} compounds present on the FTO surface followed by self-exchange "hopping" across the nanocrystalline TiO_2 surface. A moving front of oxidized dyes nearly equidistant from the FTO substrate is observed at $t > t_0$. At longer times $t \gg t_0$, all the molecules within the mesoporous thin film are oxidized. The semi-infinite diffusion boundary approximation restricts data analysis to about 60% oxidation of the thin film. In contrast, only about 5% of the film is oxidized during a cyclic voltammetry experiment.

is within experimental error the same as that measured for the analogous Ru compound, yet it is in contrast to solution phase self-exchange studies, where $[Os(bpy)_3]^{3+/2+}$ self-exchange rate constants were more than double that of $[Ru(bpy)_3]^{3+/2+}$.[26] Comparisons such as these draw attention to the differences that may exist between electron-transfer reactions between molecules in fluid solution and those anchored at a semiconductor interface. In another literature report, D_{CA} was quantified for $[Ru(bpy)_2(4,4'\text{-}(PO_3H_2)_2\text{-}bpy)]^{3+/2+}$ in a 0.1 M $HClO_4$ aqueous medium.[10] Remarkably similar values for D were quantified for this compound (1.33×10^{-9} cm^2/s) as for those reported herein. Similar values were also reported by Mallouk et al.[27] Hence, the nature of the anchoring groups, carboxylic acids versus phosphonic acids, has a less significant impact than does the inclusion of insulating organic functional groups on the ancillary ligands. However, it should be emphasized that the details of the mesoporous TiO_2 film structure may have a significant yet undocumented influence on D. Factors such as film porosity, nanocrystallite size, and surface chemistry have an unknown impact on the electron transfer kinetics. Until such parameters are better understood, systematic studies similar to the one reported here are needed.

Self-Exchange Kinetics and Theory. Estimation of the rate constant for self-exchange, k_{SE}, from D_{CV} requires knowledge of the distance between the surface anchored molecules. While it is sometimes stated that dcb-containing molecules bind to the TiO_2 surface in monolayer surface coverage, the ill-defined surface area makes such statements difficult to validate experimentally. There is little data to suggest that these dicationic complexes form multilayers on TiO_2, but whether any or all are within van der Waals radii of each other is unclear. However, in the raw measured visible absorption spectra of the thin films, it was clear that the saturation surface coverage increased in the order **dtb** < **dmb** < **bpy**. This correlates well with a steric increase in R when *tert*-butyl groups replace methyl groups or H atoms and suggests that on average the Ru centers are further apart in **dtb**.

The number of molecules present within the mesoporous film is reasonably estimated through absorption measurements using Beer's law, though the distance between the molecules

DOI: 10.1021/acs.jpcc.6b04438
J. Phys. Chem. C 2016, 120, 14226−14235

and their homogeneity is much more difficult to assess. An analysis described in the experimental section takes the total number of redox active molecules and disperses them within the mesoporous thin film as if there were no TiO_2 present, to give the largest value of R, as well as the case where the molecules pack as tightly as they do in the solid state crystal structure. These analyses provide upper and lower limits to R, that are within a factor of 10 of what would be expected when molecules as 10 Å spheres are close-packed on a planar idealized surface. Furthermore, the mean separation distance in the encounter complex formed between $Ru(bpy)_3^{3+/2+}$ for solution-phase self-exchange reaction has been calculated to be 13.6 Å which is comparable to the intermolecular distances determined from the crystal structures of the compounds.[28] The k_{SE} values abstracted in such a manner were in good agreement with previous literature reports that are discussed in more detail below.

An Arrhenius analysis of k_{SE} revealed activation energies for each studied complex were within experimental error the same, E_{act} = 250 ± 50 mV. Within the framework of Marcus theory for nonadiabatic electron transfer, the activation energy for electron transfer is approximately equal to the sum of the work required to bring the two species together and one-fourth the total reorganization energy, $\lambda/4$. Assuming the work term is zero for the reaction between anchored molecules, this activation data implies a reorganization energy of ∼1 eV, a value that is consistent with literature values for similar electron transfer reactions between Ru based chromophores anchored to TiO_2 nanocrystallites.[5] As the inner-sphere contributions to the total reorganization energy are mainly associated with the Ru−N bond lengths and angles, there was no *a priori* reason to suspect that the methyl or *tert*-butyl substituents would contribute to λ and no evidence of significant bond length alterations was evident in the crystal structures. Moreover, the structural changes observed upon oxidation of similar Ru polypyridyl complexes are minimal and therefore λ_I contribute negligibly to the total reorganization.[29] As a result, the primary contribution to the total reorganization energy arises from outer sphere contributions that are difficult to determine experimentally. On the basis of the negligible contribution of λ_I to the total reorganization energy, we conclude that the changes in steric bulk have a minimal influence on λ_O.

Application of Marcus theory using a shared λ in the fitting procedure revealed that the electronic coupling matrix element, H_{AB}, increased from 0.02 to 0.10 meV in going from **dtb** to **dmb**. A λ value of 900 ± 100 meV was found to provide the most satisfactory fit to all three data sets under the assumption that the reorganization energies do not change appreciably between the compounds investigated. In contrast to those observed here, values of H_{AB} observed for the electron self-exchange reaction for the parent complex $Ru(bpy)_3^{3+/2+}$ in fluid solution are reported to be between 2.5 and 12.4 meV.[13] The significant decrease in H_{AB} is likely a result of the increased molecular distance, and the heterogeneous nature of the interface.

Self-exchange and activation parameters garnered from studies of TiO_2|**dtb** were dramatically different than those obtained with **dmb** or **bpy**, providing compelling evidence that bulky side groups do indeed influence H_{AB}. This finding supports the previous suggestion that long-chain side groups can be used to tune self-exchange at these same interfaces. In side-by-side comparative studies, both H_{AB} and D were consistently the largest for **dmb**, which was intriguing, as this is counterintuitive to what was expected on the basis of the steric bulk of the compounds. While it is not clear why this is the case, it suggests that the electron donating behavior of the alkyl substituents is also playing a role. The self-exchange rate constants for $Ru(bpy)_3^{3+/2+}$ are orders of magnitude larger than those of the corresponding ammine or aqua compounds, behavior that Sutin rationalized by concluding that the π-acidic nature of the bipyridine provides sufficient electron density on the ligands for self-exchange.[13] It is hence likely that substituents modify the ligand electron density in a manner sufficient to alter self-exchange between immobilized redox centers.

■ CONCLUSIONS

Self-exchange intermolecular $Ru^{III/II}$ electron transfer across the surface of mesoporous nanocrystalline (anatase) TiO_2 thin film was characterized by cyclic voltammetry and chronoabsorptometry techniques for a series of three Ru polypyridyl compounds $[Ru(LL)_2(dcbH_2)](PF_6)_2$, where LL is 2,2′-bipyridine (**bpy**), 4,4′-dimethyl-2,2′-bipyridine (**dmb**)h or 4,4′-di-*tert*-butyl-2,2′-bipyridine (**dtb**) and dcb is 2,2′-bipyridyl-4,4′-dicarboxylic acid. Apparent diffusion coefficients, D, abstracted from the electrochemical data revealed that the self-exchange was much slower for the *tert*-butyl containing compounds. Temperature dependent measurements revealed that this was due to lower intermolecular electronic coupling that resulted from the sterically bulky *tert*-butyl groups. The results indicate that insulating side groups can indeed be placed on redox active molecules to tune the electronic coupling, and hence self-exchange rate constants, without significantly altering the reorganization energy for electron transfer. Such behavior can be exploited in artificial photosynthetic assemblies both to enhance and inhibit lateral charge transport across oxide surfaces.

■ ASSOCIATED CONTENT

Supporting Information

The Supporting Information is available free of charge on the ACS Publications website at DOI: 10.1021/acs.jpcc.6b04438.

Figures showing the temperature dependence of k_{SE}, UV−vis spectra generated during the oxidation of **bpy**, and spectra generated during the oxidation of **dtb**; table showing variation of R and H_{AB} using different methods of determining R; and information about single crystal X-ray crystallography (PDF)

■ AUTHOR INFORMATION

Corresponding Author

*E-mail: gjmeyer@email.unc.edu. Phone: 919-962-6320.

Present Address

∥R.M.O.: Army Research Laboratory, 2800 Powder Mill Road, Adelphi, MD 20783.

Author Contributions

§B.N.D., T.C.M.: These authors contributed equally to this work.

Notes

The authors declare no competing financial interest.

■ ACKNOWLEDGMENTS

The research is supported by the National Science Foundation (NSF) under Award CHE-1213357 and the NSF Graduate

DOI: 10.1021/acs.jpcc.6b04438
J. Phys. Chem. C 2016, 120, 14226−14235

Research Fellowship Program under Grant No. DGE-1144081 (T.C.M.). The authors would like to thank Evan E. Beauvilliers for assistance in preparing the TOC and Scheme 3.

REFERENCES

(1) Bonhôte, P.; Gogniat, E.; Tingry, S.; Barbé, C.; Vlachopoulos, N.; Lenzmann, F.; Comte, P.; Grätzel, M. Efficient Lateral Electron Transport inside a Monolayer of Aromatic Amines Anchored on Nanocrystalline Metal Oxide Films. *J. Phys. Chem. B* **1998**, *102*, 1498−1507.

(2) Heimer, T. A.; D'Arcangelis, S. T.; Farzad, F.; Stipkala, J. M.; Meyer, G. J. An Acetylacetonate-Based Semiconductor−Sensitizer Linkage. *Inorg. Chem.* **1996**, *35*, 5319−5324.

(3) Hu, K.; Meyer, G. J. Lateral Intermolecular Self-Exchange Reactions for Hole and Energy Transport on Mesoporous Metal Oxide Thin Films. *Langmuir* **2015**, *31*, 11164−11178.

(4) Trammell, S. A.; Meyer, T. J. Diffusional Mediation of Surface Electron Transfer on TiO_2. *J. Phys. Chem. B* **1999**, *103*, 104−107.

(5) Moia, D.; Vaissier, V.; López-Duarte, I.; Torres, T.; Nazeeruddin, M. K.; O'Regan, B. C.; Nelson, J.; Barnes, P. R. F. The Reorganization Energy of Intermolecular Hole Hopping between Dyes Anchored to Surfaces. *Chem. Sci.* **2014**, *5*, 281−290.

(6) Wang, Q.; Zakeeruddin, S. M.; Cremer, J.; Bäuerle, P.; Humphry-Baker, R.; Grätzel, M. Cross Surface Ambipolar Charge Percolation in Molecular Triads on Mesoscopic Oxide Films. *J. Am. Chem. Soc.* **2005**, *127*, 5706−5713.

(7) Moia, D.; Cappel, U. B.; Leijtens, T.; Li, X.; Telford, A. M.; Snaith, H. J.; O'Regan, B. C.; Nelson, J.; Barnes, P. R. F. The Role of Hole Transport between Dyes in Solid-State Dye-Sensitized Solar Cells. *J. Phys. Chem. C* **2015**, *119*, 18975−18985.

(8) Hu, K.; Robson, K. C. D.; Johansson, P. G.; Berlinguette, C. P.; Meyer, G. J. Intramolecular Hole Transfer at Sensitized TiO 2 Interfaces. *J. Am. Chem. Soc.* **2012**, *134*, 8352−8355.

(9) Hu, K.; Robson, K. C. D.; Beauvilliers, E. E.; Schott, E.; Zarate, X.; Arratia-Perez, R.; Berlinguette, C. P.; Meyer, G. J. Intramolecular and Lateral Intermolecular Hole Transfer at the Sensitized TiO_2 Interface. *J. Am. Chem. Soc.* **2014**, *136*, 1034−1046.

(10) Hanson, K.; Brennaman, M. K.; Ito, A.; Luo, H.; Song, W.; Parker, K. A.; Ghosh, R.; Norris, M. R.; Glasson, C. R. K.; Concepcion, J. J.; et al. Structure−Property Relationships in Phosphonate-Derivatized, Ru II Polypyridyl Dyes on Metal Oxide Surfaces in an Aqueous Environment. *J. Phys. Chem. C* **2012**, *116*, 14837−14847.

(11) Moia, D.; Leijtens, T.; Noel, N.; Snaith, H. J.; Nelson, J.; Barnes, P. R. F. Dye Monolayers Used as the Hole Transporting Medium in Dye-Sensitized Solar Cells. *Adv. Mater.* **2015**, *27*, 5889−5894.

(12) Penner, R. M.; Gogotsi, Y. The Rising and Receding Fortunes of Electrochemists. *ACS Nano* **2016**, *10*, 3875−3876.

(13) Sutin, N. Nuclear, Electronic, and Frequency Factors in Electron Transfer Reactions. *Acc. Chem. Res.* **1982**, *15*, 275−282.

(14) Barbara, P. F.; Meyer, T. J.; Ratner, M. a. Contemporary Issues in Electron Transfer Research. *J. Phys. Chem.* **1996**, *100*, 13148−13168.

(15) Swords, W. B.; Li, G.; Meyer, G. J. Iodide Ion Pairing with Highly Charged Ruthenium Polypyridyl Cations in CH_3CN. *Inorg. Chem.* **2015**, *54*, 4512−4519.

(16) O'Donnell, R. M.; Sampaio, R. N.; Li, G.; Johansson, P. G.; Ward, C. L.; Meyer, G. J. Photoacidic and Photobasic Behavior of Transition Metal Compounds with Carboxylic Acid Group(s). *J. Am. Chem. Soc.* **2016**, *138*, 3891−3903.

(17) Bard, A. J.; Faulkner, L. R. *Electrochemical Methods: Fundementals and Applications*, 2nd ed.; Wiley: New York, 2001.

(18) Daum, P.; Lenhard, J. R.; Rolison, D.; Murray, R. W. Diffusional Charge Transport through Ultrathin Films of Radiofrequency Plasma Polymerized Vinylferrocene at Low Temperature. *J. Am. Chem. Soc.* **1980**, *102*, 4649−4653.

(19) Marton, A.; Clark, C. C.; Srinivasan, R.; Freundlich, R. E.; Narducci Sarjeant, A. A.; Meyer, G. J. Static and Dynamic Quenching of Ru(II) Polypyridyl Excited States by Iodide. *Inorg. Chem.* **2006**, *45*, 362−369.

(20) DiMarco, B. N.; O'Donnell, R. M.; Meyer, G. J. Cation-Dependent Charge Recombination to Organic Mediators in Dye-Sensitized Solar Cells. *J. Phys. Chem. C* **2015**, *119*, 21599−21604.

(21) Ward, C. L.; O'Donnell, R. M.; DiMarco, B. N.; Meyer, G. J. Kinetic Resolution of Charge Recombination and Electric Fields at the Sensitized TiO 2 Interface. *J. Phys. Chem. C* **2015**, *119*, 25273−25281.

(22) O'Donnell, R. M.; Sampaio, R. N.; Barr, T. J.; Meyer, G. J. Electric Fields and Charge Screening in Dye Sensitized Mesoporous Nanocrystalline TiO 2 Thin Films. *J. Phys. Chem. C* **2014**, *118*, 16976−16986.

(23) Ardo, S.; Achey, D.; Morris, A. J.; Abrahamsson, M.; Meyer, G. J. Non-Nernstian Two-Electron Transfer Photocatalysis at Metalloporphyrin−TiO 2 Interfaces. *J. Am. Chem. Soc.* **2011**, *133*, 16572−16580.

(24) Li, X.; Nazeeruddin, M. K.; Thelakkat, M.; Barnes, P. R. F.; Vilar, R.; Durrant, J. R. Spectroelectrochemical Studies of Hole Percolation on Functionalised Nanocrystalline TiO 2 Films: A Comparison of Two Different Ruthenium Complexes. *Phys. Chem. Chem. Phys.* **2011**, *13*, 1575−1584.

(25) Wang, Q.; Zakeeruddin, S. M.; Nazeeruddin, M. K.; Humphry-Baker, R.; Grätzel, M. Molecular Wiring of Nanocrystals: NCS-Enhanced Cross-Surface Charge Transfer in Self-Assembled Ru-Complex Monolayer on Mesoscopic Oxide Films. *J. Am. Chem. Soc.* **2006**, *128*, 4446−4452.

(26) Chan, M.-S.; Wahl, A. C. Rate of Electron Exchange between Iron, Ruthenium, and Osmium Complexes Containing 1,10-Phenanthroline, 2,2′-bipyridyl, or Their Derivatives from Nuclear Magnetic Resonance Studies. *J. Phys. Chem.* **1978**, *82*, 2542−2549.

(27) Swierk, J. R.; McCool, N. S.; Saunders, T. P.; Barber, G. D.; Mallouk, T. E. Effects of Electron Trapping and Protonation on the Efficiency of Water-Splitting Dye-Sensitized Solar Cells. *J. Am. Chem. Soc.* **2014**, *136*, 10974−10982.

(28) Brown, G. M.; Sutin, N. A Comparison of the Rates of Electron Exchange Reactions of Ammine Complexes of ruthenium(II) and -(III) with the Predictions of Adiabatic, Outer-Sphere Electron Transfer Models. *J. Am. Chem. Soc.* **1979**, *101*, 883−892.

(29) Biner, M.; Buergi, H. B.; Ludi, A.; Roehr, C. Crystal and Molecular Structures of $[Ru(bpy)_3](PF_6)_3$ and $[Ru(bpy)_3](PF_6)_2$ at 105 K. *J. Am. Chem. Soc.* **1992**, *114*, 5197−5203.

DOI: 10.1021/acs.jpcc.6b04438
J. Phys. Chem. C 2016, 120, 14226−14235